Fragmentation analysis of ^{88}Mo* compound nucleus in view of different decay mechanisms

Neha Grover[1,*], *Bhaktima* Thakur[1], and *Manoj* K. Sharma[1]

[1]School of Physics and Materials Science, Thapar Institute of Engineering & Technology, Patiala 147004, Punjab, India

Abstract. In reference to the experimental data, the decay mechanism of ^{88}Mo* compound system formed in ^{48}Ti+^{40}Ca reaction is investigated at three beam energies (E_{beam} = 300, 450, and 600 MeV) using the collective clusterization approach of Dynamical Cluster decay Model (DCM). The calculations are done for spherical choice of fragmentation and with the inclusion of quadrupole (β_2) deformations having "optimum" orientations. According to the experimental evidence ^{88}Mo* decays via Fusion-Evaporation (FE) and Fusion-Fission (FF) processes, thus the decay cross-sections of this hot and rotating compound system are calculated for both channels. In FF decay mode, the explicit contribution of Intermediate Mass Fragments (IMF), Heavy Mass Fragments (HMF) and fission fragments (symmetric/asymmetric) is detected within DCM framework. The calculated FE and FF decay cross-sections find nice agreement with the available experimental data. Experimentally, it has been observed that the total contribution of FE and FF decay cross-sections is less than the total reaction cross-sections possibly due to the presence of some nCN component such as deep inelastic collisions (DIC), which generally contributes above critical angular momentum (ℓ_{cr}). The possibility of DIC contribution can be addressed as a future assignment in view of diminishing pocket of interaction potential above ℓ_{cr}.

1 Introduction

The quest to understand different nuclear structural properties and related dynamics has always been an interesting and challenging topic for both experimental and theoretical nuclear physicists. Heavy ion Fusion-Fission reactions have proved to be immensely useful for this purpose or to understand the exotic nature of different nuclei. Consequently, the decay of different compound nuclei formed in variety of Heavy Ion Induced Reactions (HIRs) at low energy range has become a compelling subject [1], since it helps to produce new isotopes that may not occur naturally. Moreover, such mechanisms also provide comprehensive knowledge of numerous nuclear properties and related structural and dynamical effects. Furthermore, the decay dynamics of compound nuclei having light mass ($A_{CN} \leq 90$) provide a lot of interesting opportunities, such as the exploration of competing nature of different compound nucleus mechanisms such as Fusion-Evaporation (FE; $A \leq 4$) and Fusion-Fission (FF) etc. The FF may include the contribution of Intermediate Mass Fragments (IMF; $5 < A < 20$), Heavy Mass Fragments (HMF; $20 < A < \frac{A_{CN}}{2} - 20$) and fission fragments (symmetric/asymmetric; $\frac{A_{CN}}{2} - 20 \leq A \leq \frac{A_{CN}}{2} + 20$). Here, A_{CN} represents the mass of compound nucleus and the term fragments is defined as the nuclei emitted in the decay process. Collisions or fusion processes forming the compound nucleus in the specified mass region ($A_{CN} \leq 90$) may also invite various non compound nucleus (nCN) exotic processes like Quasi Elastic (QE), Deep Inelastic Collision (DIC) processes etc. Our main focus here is to analyze FE, FF and DIC mechanisms. Deep inelastic collision is defined as the phenomenon, which maintains the partial memory of incoming channel and forms a dinuclear molecular complex system, which subsequently decays into target and projectile like fragments. It is difficult to differentiate these processes (FF and DIC) for nuclei having fissility less than businaro-gallone point [2]. Many efforts have been made by theoreticians and experimentalists to identify the DIC and FF exclusively [1, 3].

In view of above, the present work is primarily focused on the decay dynamics of compound nucleus (^{88}Mo*) formed in ^{48}Ti + ^{40}Ca reaction. Decay analysis of the above mentioned compound nucleus is worked out using the Dynamical Cluster Decay Model (DCM) [3–5] in context to the recent experimental data [6]. Calculations are done at three beam energies (E_{lab} = 300, 450, 600 MeV) by opting both spherical and β_2-deformed configuration of decaying fragments. In this work, cross-sections of both Fusion- Evaporation (FE) and Fusion-Fission (FF) decay channels are estimated. The manuscript is organized as follows: Methodology is briefly discussed in Section 2, The results and discussions are presented in the Section 3 followed by the summary in Section 4.

*e-mail: nehagrover9823@gmail.com

2 Dynamical Cluster Decay Model

The Dynamical cluster decay model (DCM) [3–5] is originated from Quantum Mechanical Fragmentation Theory (QMFT) [7].
DCM is worked out in
(i) collective coordinates of mass ($\eta_A = \frac{A_1-A_2}{A_1+A_2}$) and charge ($\eta_Z = \frac{Z_1-Z_2}{Z_1+Z_2}$) asymmetries where, 1 and 2 stand, respectively, for heavy and light fragments,
(ii) relative separation R and
(iii) multipole deformations $\beta_{\lambda i}$ ($\lambda = 2,\ 3,\ 4$) and orientations θ_i of two nuclei or fragments. For decoupled Hamiltonion, the Schrödinger wave equation in η co-ordinate reads as:

$$\left[-\frac{\hbar^2}{2\sqrt{B_{\eta\eta}}}\frac{\partial}{\partial\eta}\frac{1}{\sqrt{B_{\eta\eta}}}\frac{\partial}{\partial\eta} + V_R(\eta,T)\right]\psi^{\nu}(\eta) = E^{\nu}_{\eta}\psi^{\nu}(\eta). \quad (1)$$

where $\nu = 0,1,2...$ refers to ground, first and second state solutions respectively and $B_{\eta\eta}$ is smooth hydrodynamical mass parameter.

The fragmentation potential $V_R(\eta, T)$ in Eq.1 is calculated by summation of (i) V_{LDM} (T-dependent liquid drop energy of Davidson [8]) with its constants at T = 0 refitted [9] to give the experimental binding energies [10], (ii) δU, the empirical shell corrections of Myers and Swiatecki [11] and (iii) V_C, V_P and V_ℓ are, respectively, T-dependent Coulomb, nuclear proximity and angular momentum dependent potentials for deformed and oriented nuclei. The expression for $V_R(\eta, T)$ is given as:

$$V_R(\eta,T) = \sum_{i=1}^{2}[V_{LDM}(A_i,Z_i,T)] + [\sum_{i=1}^{2}[\delta U_i]\times \exp(-T^2/T_0^2)] + V_C + V_P + V_\ell. \quad (2)$$

The formation yield of decaying fragments is worked out by calculating preformation factor (P_0) as solution of Eq.1 and the equation for P_0 is given as:

$$P_0 = |\ \psi(\eta(A_i))\ |^2\ \sqrt{B_{\eta\eta}}\frac{2}{A_{CN}}. \quad (3)$$

The preformation factor (P_0) shown in Eq.3 refers to η-motion. In tunneling process, the barrier penetrability "P" of clusters or fragments refers to R motion and is calculated by using the Wenzel-Kramers-Brillouin (WKB) integral as:

$$P = \exp\Big[-\frac{2}{\hbar}\int_{R_a}^{R_b}\{2\mu[V(R)-Q_{eff}]\}^{1/2}dR\Big] \quad (4)$$

where, $R_a = R_1(\alpha_1,T) + R_2(\alpha_2,T) + \Delta R(T) = R_i(\alpha_i,T) + \Delta R(T)$ is the first turning point of the barrier penetration with ΔR as relative separation distance between two fragments or clusters. ΔR is the only parameter of model, which is optimized in reference to the available data. It decides the first turning point of barrier penetration and $R_i(\alpha_i, T)$(i=1,2) is radius vector defined as:

$$R_i(\alpha_i,T) = R_{0i}(T)\Big[1 + \sum_{\lambda}\beta_{\lambda i}Y^{(0)}_{\lambda}(\alpha_i)\Big]. \quad (5)$$

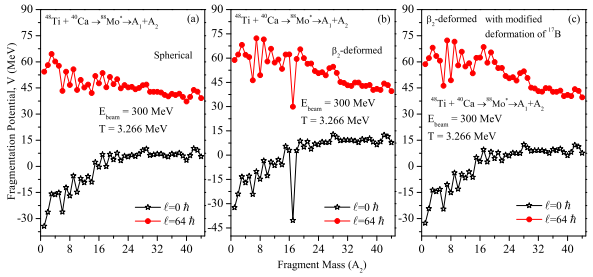

Figure 1. Fragmentation potential with respect to the fragment mass for ^{48}Ti+^{40}Ca→ ^{88}Mo* reaction at extreme ℓ-values ($\ell = 0$ & 64) for the spherical and β_2-deformed fragments in exit channel.

where $\beta_{\lambda i}$ represents static deformations and are taken from the theoretical estimates of Moller and Nix [12] and R_{0i}(T) in Eq.5 is T-dependent nuclear radius as per ref. [13].
By calculating P and P_0, the decay cross-sections are calculated as:

$$\sigma = \sum_{\ell=\ell_{min}}^{\ell_{max}}\sigma_\ell = \frac{\pi}{k^2}\sum_{\ell=\ell_{min}}^{\ell_{max}}(2\ell+1)P_0P. \quad (6)$$

where, $\mu = [A_1A_2/(A_1+A_2)]m$ is the reduced mass, ℓ_{min} and ℓ_{max} are the minimum and maximum angular momentum respectively and $k = \sqrt{\frac{2\mu E_{c.m.}}{\hbar^2}}$.

For CN mechanisms such as FE and FF, the ℓ-window contributing towards decay is $0 \le \ell \le \ell_{cr}$ and for nCN process viz. DIC it is $\ell_{cr} < \ell \le \ell_{gr}$. ℓ_{cr} is that (critical) value of angular momentum above which compound nucleus formation is hindered and the grazing angular momentum (ℓ_{gr}) is the upper limit of partial wave above ℓ_{cr}-value upto which, the contribution of nCN peripheral collisions be explored. The values of ℓ_{cr} and ℓ_{gr} used in present study at respective energies are taken in reference to [6].

3 Results and discussions

This section presents the DCM-calculated results for different decay modes of ^{88}Mo* composite system formed in ^{48}Ti + ^{40}Ca reaction. First, to study the role of deformations, two choices of fragmentation paths (spherical and β_2-deformed) are considered. Fig. 1 shows the variation of fragmentation potential V(A_2) as a function of fragment mass for the decay of ^{88}Mo* at lowest energy E_{lab} = 300 MeV. It is important to mention here that A_1 and A_2 in ^{48}Ti + ^{40}Ca → ^{88}Mo* → $A_1 + A_2$ subtitle represent the decaying fragments, which may belong to any of the possible compound nucleus decay modes (FE, IMF, HMF, Fission). Here, it is worth mentioning that the fragments having minima in $V_R(\eta)$ are most probable candidates in the exit channel as they require lesser potential to penetrate the barrier. It is clearly evident from Fig. 1 that the emission of light particles is dominant at $\ell = 0\,\hbar$ for both spherical and deformed choices of fragments. However, with the increase in ℓ-values, the

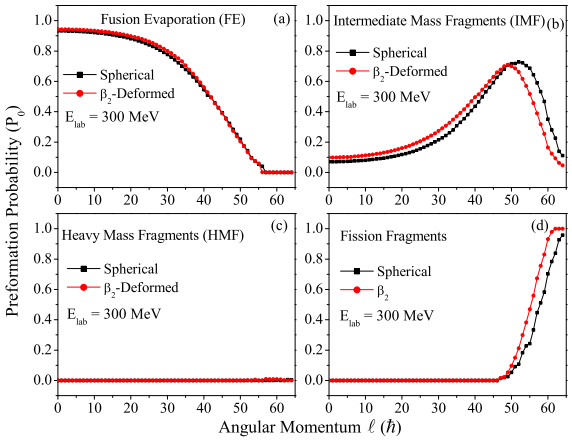

Figure 2. Summed up preformation probability of all possible decay modes: (a) FE, (b) IMF, (c) HMF, and (d) fission, varying as a function of angular momentum (ℓ) for both spherical and β_2-deformed choice of fragments at $E_{lab} = 300$ MeV.

Table 1. Fusion-Evaporation (FE) and Fusion-Fission (FF) cross-sections for ^{48}Ti + ^{40}Ca → ^{88}Mo* reaction at three given beam energies calculated using DCM and compared with the experiment data [6]

S. No.	E_{lab} (MeV)	$E_{c.m.}$ (MeV)	Temp. (MeV)	Spherical ΔR (fm)	Spherical σ_{DCM} (mb)	β_2-deformed ΔR (fm)	β_2-deformed σ_{DCM} (mb)	$\sigma_{Exp.}$ (mb)
				Fusion-Evaporation (FE)				
1	300	136.36	3.27	1.86	848	1.85	859	893±109
2	450	204.54	4.05	2.00	569	1.95	521	545±45
3	600	272.73	4.70	2.18	475	2.10	412	459±115
				Fusion-Fission (FF)				
1	300	136.36	3.27	1.36	121	1.39	111	115±3
2	450	204.54	4.05	1.62	245	1.67	261	266±37
3	600	272.73	4.70	1.89	383	1.94	388	417±114

value of $V_R(\eta)$ for fission region start comparing with FE channel, which signifies the prominence of fission fragments at higher values of angular momentum. In other words, Fusion Fission (FF) starts operating at the cost of FE at higher ℓ-values. Further, moving towards the influence of deformations, it may be noticed from Fig. 1(b) that the structure profile remains almost similar for both cases of fragmentation except for a sharp minima at ^{17}B for deformed choice of fragmentation. Interestingly, similar results were observed for the decay of ^{96}Tc* nucleus in ref. [4], which state that this abrupt minima at ^{17}B might be due to inappropriate β_2-deformation of this fragment. It is relevant to note that β_2-deformations are taken from Moller and Nix [12], where certain values are obtained after interpolations and extrapolations and hence there exists a possibility that β_2-values of certain fragments may not be accurate. Thus to rectify this problem, modified β_2-deformation of ^{17}B is used as per ref. [4], and the results are presented in Fig. 1(c), which exhibit the expected behavior of fragmentation potential. Consequently, further calculations are made using modified β_2-deformation for ^{17}B fragment (i.e

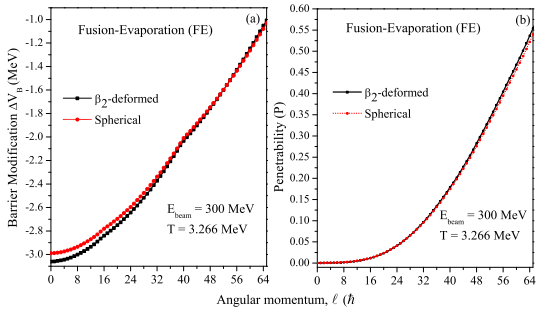

Figure 3. The variation of (a) barrier modification (ΔV_B) and (b) Penetrability, P as a function of angular momentum (ℓ) for Fusion-Evaporation channel at $E_{lab} = 300$ MeV for ^{88}Mo* nucleus.

$\beta_2 = 0.620$). Similar results are obtained at maximum energy, $E_{lab} = 600$ MeV (not shown here to avoid repetition). As the fragmentation potential works as an essential input in Schrodinger Equation (Eq. 1), solution of which defines the preformation probability (P_0) of fragments participating in the exit channel. This preformation factor confers significant structural information of compound nucleus that otherwise does not exist in other statistical models.

To investigate the probability of different decay modes participating in the exit channel, the variation of summed up preformation probability (ΣP_0) with respect to angular momentum is plotted for possible decay channels: FE, IMF, HMF, and fission and the results are displayed in Fig. 2 at $E_{lab} = 300$ MeV for both spherical and β_2-deformed fragmentation paths. One may clearly see from Fig. 2(a) that for both spherical and deformed case, the preformation probability of FE is maximum for a particular ℓ-window ($0 \le \ell \le 20\,\hbar$) and then decreases gradually and becomes almost negligible at higher ℓ-values. The ΣP_0 for IMF region is presented in Fig. 2(b). The figure illustrates that ΣP_0 is approximately zero up to $\ell \approx 15\,\hbar$ and then attains the maximum value at higher ℓ-values before reducing to zero at ℓ_{max}. By comparing Fig. 2(a) and (b), it can be affirmed that the FE is more probable at lower ℓ-values and at higher ℓ-window IMF start competing with FE component. Furthermore, panel (c) of Fig. 2 shows that the contribution of HMF in the decay of ^{88}Mo* is negligibly small at all ℓ-values. Finally, ΣP_0 for the fission region is plotted in panel (d) of Fig. 2, which suggest that fission component appears at higher ℓ-values. Concluding the analysis of Fig. 2, one may say that FE is the most dominant decay mode among the four possibilities considered here. It is relevant to note that, the cross-sections for FE and FF are addressed by optimizing the neck length parameter (ΔR) "the only parameter of DCM" and the results are tabulated in Table 1. It is clearly evident from the table that the DCM calculated cross-sections are in good agreement with the experimental data [6]. Moreover, the neck parameter used

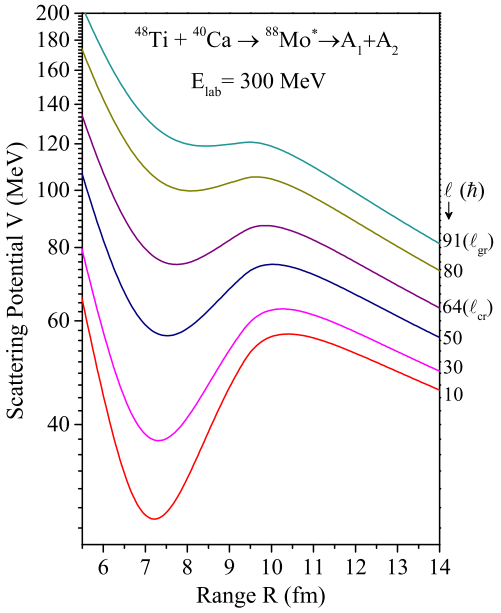

Figure 4. Variation of interaction potential V(R) (sum of V_P, V_C and V_ℓ) as function of range at different ℓ-values for β_2-deformed choice of fragments.

to address the cross-sections leads to the corresponding barrier modification ($\Delta V_B(\ell) = V(R_a, \ell) - V_B(\ell)$), which is an in-built property of DCM and plays very crucial role to fix the tunneling path of decaying fragments. Fig. 3 demonstrates the behavior of ΔV_B (panel-a) and penetrability (panel b) as a function of angular momentum for fusion evaporation channel. One may clearly notice from the Fig. 3(a) that, the magnitude of ΔV_B is higher at lower ℓ-values and decreases with the rise in angular momentum. This signifies that to tunnel the barrier at higher angular momentum, the required barrier modification is less in comparison to that at lower ℓ-values. As a consequence, the penetrability also increases with the increment in angular momentum, as evident from Fig. 3(b). Similar results are obtained for fusion-fission channel (not shown here).

3.1 Future Work

It is claimed [6] that the decay of ^{88}Mo* formed via ^{48}Ti + ^{40}Ca reaction, might include the Deep Inelastic Collision (DIC; nCN component) along with FE and FF. Thus, an attempt is made to analyse the same by plotting interaction potential as a function of range for different ℓ-values ($0 < \ell_{cr} \leq \ell_{gr}$) in Fig. 4. It is evident from the figure that with increase in angular momentum, pocket of potential barrier becomes more shallow but still exist upto critical angular momentum. However at $\ell > \ell_{cr}$, the barrier starts vanishing with rise in angular momentum and almost disappears at grazing angular momentum (ℓ_{gr}). The disappearance of barrier pocket near grazing angular momentum indicates the possible presence of DIC at higher ℓ-values. Thus, it would be of future interest to address the DIC cross-sections for the present reaction as a future assignment.

4 Summary

Summarizing, the present work employs the decay analysis of ^{88}Mo* compound system formed in ^{48}Ti+^{40}Ca reaction at three beam energies (E_{lab} = 300, 450 and 600 MeV). Firstly, the inclusion of deformation effects depict that the structural profile of fragmentation potential remains similar for both the spherical and β_2-deformed choice of fragments, which implies that the deformations do not play significant role in decay dynamics of ^{88}Mo* nucleus. The competing analysis of four different decay modes FE, IMF, HMF and fission reveals that, the FE is the most dominant decay channel and HMF has negligible contribution in the decay of ^{88}Mo*. It is observed that lesser barrier modification is required at higher ℓ-values for all decay modes. Consequently, penetrability increases with increase in angular momentum. The DCM calculated cross-sections are inline with the experimental data. Additionally, as per the experimental evidence, an attempt is also made to advocate the presence of nCN process. It is observed that the pocket of potential barrier becomes shallower at higher values of angular momentum and almost disappear above critical angular momentum, which indicates the presence of nCN component such as DIC. It would be of future interest to analyse the nCN component associated with such reactions.

Acknowledgements

The financial support from the UGC-DAE Consortium for Scientific Research, F. No. UGC-DAE-CSR-KC/CRS/19/NP09/0920 is gratefully acknowledged.

References

[1] S. J. Sanders, D. G. Kovar, B. B. Back *et al.*, Phys. Rev. C **40**, 2091 (1989); S. J. Sanders, B. B. Back, R. V. F. Janssens *et al.*, Phys. Rev. C **41**, R1901 (1990).
[2] C. Beck, B. Djerroud, B. Heuseh *et al.*, Z. Phys. A **334**, 521 (1989).
[3] N. Grover, K. Sharma, and M. K. Sharma, Eur. Phys. J. A **53**: 239 (2017).
[4] G. Kaur, N. Grover, K. Sandhu *et al.*, Nucl. Phys. A **927**, 232–248 (2014).
[5] R. K. Gupta, M. Balasubramaniam, R. Kumar *et al.*, Phys. Rev. C **71**, 014601 (2005).
[6] S. Valdré, S. Piantelli, G. Casini *et al.*, Phys. Rev. C **93**, 034617 (2016).
[7] J. Marhun and W. Greiner, Phys. Rev. Lett. **32**, 548 (1974).
[8] N. J. Davidson, S. S. Hsiao, J. Markram *et al.*, Nucl. Phys. A **570**, 61c (1994).
[9] B. B. Singh, M. K. Sharma, and R. K. Gupta, Phys. Rev. C **77**, 054613 (2008).

[10] G. Audi, A. H. Wapstra, C. Thiboult, Nucl. Phys. A **729**, 337 (2003); G. Audi, A. H. Wapstra, Nucl. Phys. A **595**, 4 (1995).
[11] W. Myers, W. J. Swiatecki, Nucl. Phys. **81**, 1 (1966).
[12] P. Möller, J. R. Nix, W. D. Myers *et al.*, At. Data Nucl. Data Tables **59**, 185 (1995).
[13] G. Royer and J. Mignen, J. Phys. G: Nucl. Part. Phys. **18**, 1781 (1992).